Interaction between caesium iodide particles and gaseous boric acid in a flowing system through a thermal gradient tube (1030 K–450 K) and analysis with ASTEC/SOPHAEROS

Gouello, Melany; Hokkinen, Jouni; Suzuki, Eriko; Horiguchi, Naoki; Barrachin, Marc; Cousin, Frédéric

Published in:
Progress in Nuclear Energy

DOI:
10.1016/j.pnucene.2021.103818

Published: 11/06/2021

Document Version
Publisher's final version

Progress in Nuclear Energy 138 (2021) 103818

Contents lists available at ScienceDirect

Progress in Nuclear Energy

journal homepage: www.elsevier.com/locate/pnucene

Interaction between caesium iodide particles and gaseous boric acid in a flowing system through a thermal gradient tube (1030 K–450 K) and analysis with ASTEC/SOPHAEROS

Mélany Gouëllo [a,*], Jouni Hokkinen [a], Eriko Suzuki [b], Naoki Horiguchi [b], Marc Barrachin [c], Frédéric Cousin [c]

[a] VTT Technical Research Centre of Finland Ltd, P.O. Box 1000, FI-02044, VTT, Finland
[b] Nuclear Science and Engineering Center, Japan Atomic Energy Agency, 2-4 Shirakata, Tokai-mura, Naka-gun, Ibaraki, 319-1195, Japan
[c] IRSN Institut de Radioprotection et de Sûreté Nucléaire, PSN-RES/SAG/LETR, BP3, 13115, St. Paul Lez Durance, France

ARTICLE INFO

Keywords:
Caesium iodide
Boric acid
Primary circuit
NUCLEA
ASTEC/SOPHAEROS analysis
CHASER

ABSTRACT

The present work aimed at studying the interaction between caesium iodide particles and gaseous boric acid through a Thermal Gradient Tube (TGT) from 1023 K to 453 K under Ar/H_2O. Particles size range of transported particles was measured by ELPI and the fraction of gaseous compounds by ICP-MS and UV–visible spectroscopy. Reaction between the two compounds was deduced by measuring a significant fraction of gaseous iodine at the outlet of the facility, representing more than 80% of the total iodine sampled at the outlet. The reaction rate was shown to be lower when the flow rate inside the facility was increased. Analysis with SOPHAEROS module of ASTEC code was performed. The ASTEC fission products models allowed performing the evaluation of the experimentally observed results for the analysis of the transport of pure compounds. However, the heterogeneous interaction between the caesium iodide particles and the gaseous boric acid was not reproduced, as the models are not taken into account in the version v2.1_1_6 of the ASTEC/SOPHAEROS module. The next step would be to identify the mechanism of the reaction by comparing the results with other studies and to determine the reaction rates. Then, a first development in SOPHAEROS would be to implement such phenomena.

1. Introduction

Since the Fukushima Dai-Ichi (1 F) Nuclear Power Station accident, a renewed attention has been posed on boron carbide (B_4C) control rods. It is suspected that the core and the boron carbide control rod materials melted (Tanabe, 2011) and relocated downward to the lower plenum. The relocated melt and the boron carbide material would be then oxidized in contact with steam, leading to a release of boron-containing gaseous species (Haste et al., 2012; Miwa et al., 2016). Depending on the accident scenario, the boron species can then react with fission products (gas, vapour and/or aerosols) and consequently affect the source term.[1]

The Phébus Fission Products (FP) tests[2] revealed that the boron can indirectly enhance the amount of gaseous iodine released into the containment building. Indeed, the use of a boron carbide control rod in FPT-3, in replacement of Ag–In–Cd,[3] was proposed to explain the formation of gaseous iodine forms (Barrachin et al., 2013; Girault and Payot, 2013; Haste et al., 2012; T Haste et al., 2013). The percentage of gaseous iodine measured at the break (from less than 1% up to several tens of % (Cantrel et al., 2013)) was revealed by the sensitivity analysis carried out with ASTEC, to have an impact on the source term (Cousin et al., 2011). In addition, a large partial boron-rich blockage between the hot and cold legs was deduced in FPT-3 (T Haste et al., 2013; T. Haste et al., 2013). In this part of the Reactor Coolant System (RCS), the temperature fell from 970 K to 420 K.

Considered as the main iodine species entering the RCS in severe accident (Soffer et al., 1995), caesium iodide has been subject of several

* Corresponding author.
E-mail address: melany.gouello@vtt.fi (M. Gouëllo).

[1] The source term is defined as the magnitude, the chemical and physical form of the fission product source distribution in the containment atmosphere, during severe accident conditions (Sehgal, 2001).

[2] The Phébus-FP facility is an experimental reproduction of a Loss Of Coolant Accident (LOCA) at one-five thousandths scale.

[3] Ag–In–Cd control rods were used in FPT-0, FPT-1 and FPT-2.

https://doi.org/10.1016/j.pnucene.2021.103818
Received 29 September 2020; Received in revised form 24 May 2021; Accepted 3 June 2021
Available online 11 June 2021

studies to understand its behaviour, in particular in presence of boron.

Regarding the homogeneous reaction between the species in gaseous phase, work performed at the Institute for Radiological Protection and Nuclear Safety (IRSN) in a TGT (1830 K–420 K; Ar/H_2O 20/80 vol%) (Gouëllo et al., 2012) and on-going tests at the Japan Atomic Energy Agency (JAEA) in a TGT (1000 K–400 K; Ar/H_2O 80/20 vol%) (Miyahara et al., 2020) have underlined the high reactivity between the compounds, leading to the formation of gaseous iodine and its transport at 420 K.

Reaction between caesium iodide and boron oxide in condensed phase, studied under several atmosphere compositions (Ar/H_2O, Ar/H_2O/H_2 and Ar/Air) from 670 K to 920 K, has also revealed to lead to the formation of gaseous iodine, mostly molecular iodine, and caesium borates (Gouëllo et al., 2018).

The investigations of the interactions in heterogeneous phase (gas/condensed phases) in a TGT have been initiated in 1990s at the United Kingdom Atomic Energy Authority (Bowsher et al, 1985, 1986). Authors observed that boric acid can react with a part of caesium iodide, leading to the release of gaseous iodine.

In the framework of the WIND (Wide Range Piping Integrity Demonstration) project at the Japan Atomic Energy Research Institute (JAERI) (Shibazaki et al., 2000), reactivity between caesium iodide particles deposited onto the surfaces of a TGT (1270 K–640 K) and a metaboric acid layer placed beforehand, was noticed. Deposited caesium iodide was mostly decomposed at the temperature exceeding approximately 770 K.

The past work brought a lot of information on the reactions between caesium iodide and boric acid in a TGT, broadening the database in several conditions and demonstrating how presence of boric acid can affect the physical and chemical forms of iodine and caesium, in particular through the formation of stable condensed caesium borates ($Cs_xB_yO_z$) (Vandeputte et al., 2019). However, no test was carried out with the aim of studying the reactivity between particles of caesium iodide in suspension and gaseous boric acid. Considering the concentration of particles and the large specific area it provides for condensation of vapours and reaction, it can lead to a higher reactivity than caesium iodide deposited/condensed on the RCS walls.

In this context, the first focus in this study was to determine the caesium iodine particles transport through a TGT and then to assess the effect of gaseous boric acid with the suspended particles.

Concurrently, the need for a better method for predicting source term under severe accidents in Light Water Reactor (LWR) has been raised, especially regarding to the iodine and caesium behaviours, which are subject to uncertainties (Di Giuli et al., 2016; Nowack et al., 2018). In addition to determining if the interaction between gaseous boric acid and suspended caesium iodide particles may be relevant enough to affect the source term, this study will provide data, which will be used for the validation of accident analysis codes or for the implementation of the observed phenomena in models.

The selected approach is first to acquire data on the effect of possible reaction between gaseous boric acid and caesium iodide particles in a flowing gas. The number and mass concentrations of particles in suspension at the outlet of the TGT under Ar/H_2O (80/20 vol%) and the amount of gaseous iodine transported to the sampling lines at 450 K will be measured. The second part of the work consists in validating the models implemented in the SOPHAEROS module (version v2.1_1_6) of the Accident Source Term Evaluation Code (ASTEC) (Cousin et al., 2008) on the basis of a comparison with the obtained experimental results.

2. Material and methods

2.1. EXSI-AERIS facility

A schematic figure of the experimental EXSI-AERIS facility is presented in Fig. 1. The main component of the facility was the horizontal tube furnace (Entech ETF 30/12), used to heat up more than half[4] of the pre-oxidized stainless steel TGT (AISI 304, outside diameter 28 mm and 750 mm length provided by Restek Corporation®). The furnace (height: 550 mm; width: 440 mm; depth: 270 mm) had one heating section (300 mm long). At both ends of the furnace, there was 70 mm of thermal insulation. The tube has been pre-oxidized at 1273 K for 3h30 in pure steam atmosphere (4.2 l/min) (Gouëllo et al., 2020), and a new tube is used for each experiment.

The caesium iodide aerosols were generated by nebulization of a concentrated caesium iodide aqueous solution (see section 2.4) and were introduced upstream from the main stainless steel tube by a stainless steel line heated at 373 K. The generated particles were led directly to the high-temperature zone (1030 K) by a stainless steel tube (diameter: ¼ in), avoiding then interaction with generated boric acid upstream the TGT. The boric acid (H_3BO_3) (99.97% trace metals basis provided by SigmaAldrich®) was generated by vaporization from an alumina crucible placed at the entrance of the furnace. By weighing the crucible with the powder before and after the test, an average vaporization mass flow rate of boric acid feed could be estimated to vary between 1.6 and 1.9 mg/min (see Table 2).

The carrier gas, a mixture of argon and steam, was passed through the system. The measured thermal profile is presented in Fig. 2. During the test, the fluid and wall temperatures were measured at several points in the facility (Fig. 1).

In the sampling furnace, the main flow was split into four lines:

(1) A line was directed to a Fourier Transform Infrared spectrometer (FTIR), which monitored the percentage of steam during the test.
(2) A second line headed for aerosol on-line measurement. Upstream from the online aerosol measurement devices, the flow was diluted with a porous tube diluter (dilution factor of 21) in order to decrease the concentration of the produced particles low enough for the instrumentation as well to decrease the temperature of the flow below 313 K.
(3) A third line was used to sample particles and gaseous species. The line was equipped with a polytetrafluroethylene (PTFE) membrane filter (hydrophobic, poral grade 5.0 μm, 47 mm, Mitex®) and two liquid traps assembled in series. The liquid traps were filled with an immiscible solution composed of aqueous phase (nitric acid, pH = 3; 50 ml) and an organic phase (toluene; 100 ml) in order to selectively separate hydrogen iodide (HI) from molecular iodine (I_2). Due to its non-polarity, molecular iodine is expected to be trapped in the organic phase while hydrogen iodide would stay in the aqueous phase. This line was used for the first 20-min sampling (S1). The quantification of molecular iodine in toluene was carried out by UV–visible spectroscopy.
(4) A fourth line was used, with a similar configuration as the third line, except the nature of the liquid traps. They were filled with a solution of 0.1 M sodium hydroxide (NaOH) and 0.02 M sodium thiosulfate ($Na_2S_2O_3$) (150 ml) in water. After the test, the solutions and the leachants from filters (50 ml) were analysed by Inductively Coupled Plasma Mass Spectrometry (ICP-MS). This line was used for the second 20-min sampling (S2).

2.2. Caesium iodide aerosol generator

Although, in FPT-3, a low iodine aerosol amount[5] was measured in the hot leg point (Girault and Payot, 2013), the caesium was mainly

[4] The tube was placed as follow inside the furnace: upstream 10 mm of the tube was outside the furnace, then 440 mm was inside the furnace, and 300 mm of the tube was downstream, not heated by the furnace and only insulated by Isofrax 1260C.

[5] At the hot leg point (named point C), during FPT-3, about 62% of iodine was under gas or vapour form (Cantrel et al., 2013).

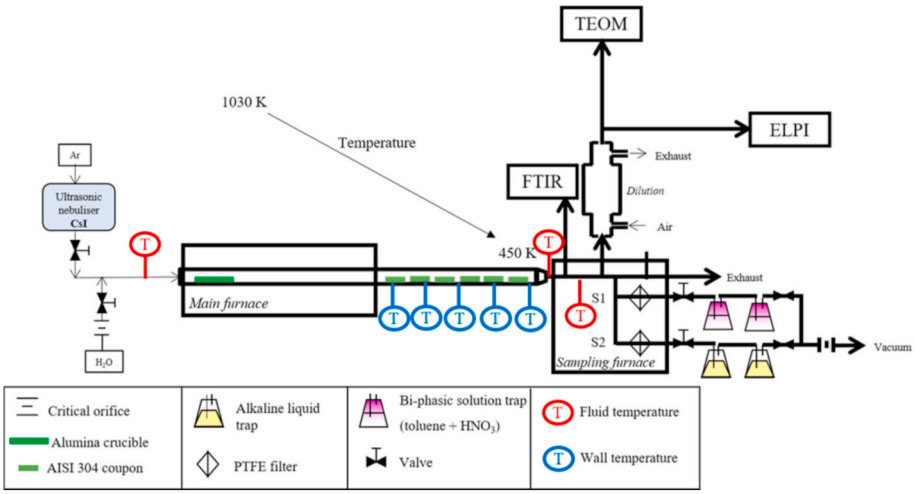

Fig. 1. Schematic figure of the experimental EXSI-AERIS facility.

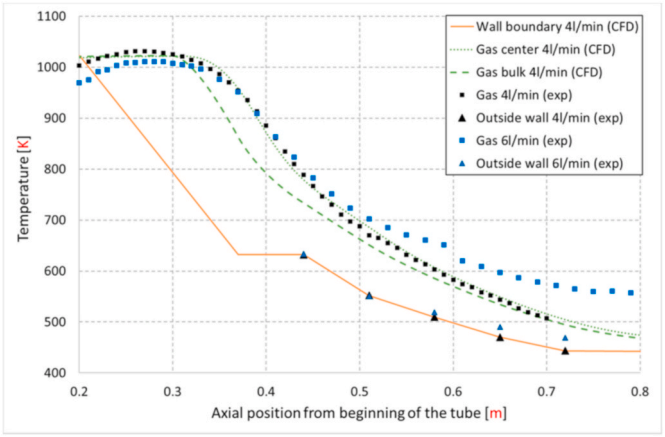

Fig. 2. Thermal profile in the TGT for a carrier gas composed of Ar/H_2O (80/20 vol%.) and a flow rate of 4 l/min and for a carrier gas composed of Ar/H_2O (82/18 vol%.) and a flow rate of 6 l/min.

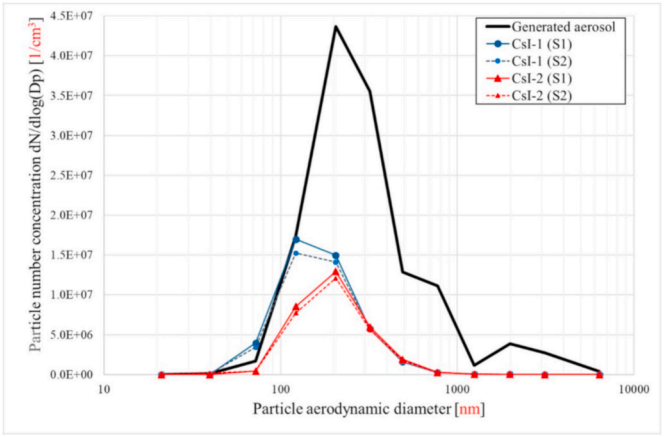

Fig. 3. Number concentration of caesium iodide particles obtained from the nebulization of caesium iodide solution (1 g/l) in black and particles transported through the TGT as a function of the particle aerodynamic diameter (Dp) recorded with ELPI.

observed in aerosol form (Haste et al., 2011), it was decided to introduce caesium iodide in the form of particles at 1023 K, temperature assessed at the hot leg break, and to investigate the possible reactivity of those particles with boric acid.

The particles were generated by nebulization of a concentrated caesium iodide aqueous solution (1 g/l of caesium iodide powder 99.9 wt%, provided by SigmaAldrich®) at room temperature and atmospheric pressure. The ultrasonic nebulizer uses mechanical forces from an oscillating transducer to break a liquid sample stream into very small droplets with a relatively uniform droplet size. The nebulizer was qualified and it was chosen to work with a value on the nebulizer control box of 5.5 and an argon flow of 1.4 l/min, generating aerosols with the particle number size distribution presented in a thick black curve on Fig. 3. The generated particles were in the range of the particles size reported at the hot leg during the Phébus FPT-3 (Haste et al., 2011). Indeed, the hot leg impactor deposits showed predominantly ball-shaped aerosol particles, with diameters typically ranging from 100 to 2000 nm (Haste et al., 2011). As only elementary analyses[6] were conducted on the impactor deposits, the size of the caesium iodide particles transported in the RCS during Phébus FPT-3 could not be determined specifically. The average number concentration determined by ELPI was $2.6 \cdot 10^7$ 1/cm^3. The Aerodynamic Median Diameter was 250 nm. The average mass concentration determined by TEOM was 48.5 mg/m^3. The mass flow rate of CsI would then be 0.194 mg/m^3.

2.3. Experimental conditions and matrix of tests

Fission products and structural materials face a changing environment during their transport through the RCS during severe accident. The carrier gas, composed of steam and hydrogen, can be characterized by chemical composition from oxidizing to reducing and velocities range from 0.001 to 1.0 m/s (Honaiser, 2003). From a temperature of nearly 1873 K at the entrance of the RCS, the gas cools down to 1023 K and 423 K, respectively at the hot leg and cold leg break before entering into the containment building. The pressure of the RCS can range from operational pressure to atmospheric pressure (Sehgal, 2011).

In the present study, the absolute pressure in the facility was fixed at $1 \cdot 10^5$ Pa. Gas flow rate was set under Standard Temperature and Pressure (STP). The carrier gas was a mixture of argon and steam (Table 1). Argon flow rate was controlled with a mass flow controller (Brooks S5851). A VEIT steam generator (model 2365 operates at 6.6 kW/5 bar constant output pressure) was used to generate steam. The

[6] The impactor deposits were analysed by gamma-ray spectrometry, Energy Dispersive Spectroscopy (EDS) and Inductively Coupled Plasma Mass Spectrometry (ICP-MS).

Table 1
Test matrix.

	CsI-1	CsI-2	B-1	B-2	B-3
Injected species	CsI	CsI	H_3BO_3	CsI + H_3BO_3	CsI + H_3BO_3
Atmosphere composition (vol %)	Ar/H_2O (80/20)	Ar/H_2O (80/20)	Ar/H_2O (80/20)	Ar/H_2O (80/20)	Ar/H_2O (82/18)
Total flow rate [l/min](NTP)	4	4	4	4	6

flow rate was controlled using two different critical orifices; steam volume flow rates of 0.8 l/min and 1.1 l/min (calculated at 373 K) were obtained.

For the studied flow rate reported in Table 1, the residence times of the species in the transport zone (i.e. from the high temperature zone to TGT outlet) were about 3.3 s and 2.2 s. This is in the range of the residence times, which can be calculated in RCS down to the cold leg break in the LOCA scenario (gas residence time of 2–6 s for instance for FPT0 and FPT1 (Cantrel and Krausmann, 2003)). The Reynolds numbers calculated for the different conditions are representative of a laminar flow inside the TGT (355 and 533).

Two reference tests with caesium iodide (CsI-1 to CsI-2) and one reference test with boric acid (B-1) have been performed to study the behaviour of the compound separately in the TGT. Finally, two tests were conducted in presence of caesium iodide particles and gaseous boric acid (B-2 to B-3). Table 1 indicates the test matrix.

2.4. Analytical methods

The percentage of steam at the inlet of the facility was determined by the Gasmet Dx4000 FTIR.

The aerosol mass concentration was monitored by Tapered Element Oscillating Microbalance Series 1400a (TEOM). It distinguishes itself from other particulate matter monitoring system by utilizing a direct mass measurement that is not subject to measurement uncertainties found in other surrogate technologies. Data were taken from the analog output, which was run with a range of −100 to +200 mg/m^3 to avoid truncating negative instrument responses. The filter sample flow rate (1 l/min) and temperature (300 K) were used. All TEOM data are reported at standard temperature and pressure. The measurement and the function of the instrument were monitored with RPComm software version 2.1.0. The manufacturer specifies precision of the 1400a as ±1.5 μg/m^3 (1 h average) or ±0.5 μg/m^3 (24 h average). Additionally, the mass measurement accuracy of the instrument is specified by the manufacturer as ±0.75% (Thermo Fisher, 2009).

The particle number size distribution was measured with an Electrical Low-Pressure Impactor (ELPI) (Classic ELPI®, Dekati Ltd model 97 2 E) with a time resolution of 1 s. As described in (Kärkelä et al., 2017), particles were charged with a corona charger and then differentiated by their aerodynamic diameter on twelve impaction stages inside the cascade impactor. The aerodynamic diameter is defined as the diameter of a spherical particle with a density of 1 g/cm^3 that has the same settling velocity as the measured particle (Hinds, 1999). The number concentration of particles on each impaction stage was derived from the electrical charge of particles and the measured electrical current from the stages. The inlet of the impactor was at atmospheric pressure and the outlet was at 10^4 Pa (absolute). The flow rate through ELPI was 9.29 ± 0.20 l/min (NTP). The measurement range of the ELPI was from ca. 7 nm to 10 μm. The measurement uncertainty was ±10%. The data are plotted on a lognormal X-axis.

The concentration of molecular iodine in toluene was determined using a PerkinElmer spectrophotometer model Lambda 900. In toluene, the absorption curve of molecular iodine presents two peaks at 306 nm and 497 nm, giving respective molar extinction coefficients of 7901.0 l mol^{-1}·cm^{-1} and 1064.8 l mol^{-1}·cm^{-1}. The LOD of iodine in toluene was estimated to be $8.0 \cdot 10^{-8}$ mol/l with a 10-cm glass cuvette. The measurement uncertainty was ±10%.

The leaching solutions of the filters[7] containing the transported aerosol particles transported to the liquid traps and the liquid traps were analysed using ICP-MS. The analyses were performed with a Thermo Fisher Scientific HR-ICP-MS Element 2 apparatus. The solutions were diluted into sodium hydroxide solution (0.1 M) prior to the analysis. The iodine and caesium standards and controls, 0.5, 1, 10, 20 and 100 ppb, were diluted from the Reference Standard solutions (iodine: Inorganic Ventures CGICI1; caesium: Inorganic Ventures IV-STOCK-21; boron: SPEX CertiPrep Claritas PPT® CLMS-4). All measured solutions contained an internal standard; 10 μg/l of rhodium, to control the changes in signal. The samples were injected through PFA μflow nebulizer and double pass spray chamber equipped with Peltier cooling unit. Washing

Table 2
Transported amounts of iodine, caesium and boron in the tests, calculated from the filter and liquid trap samples (analysed with ICP-MS) and aerosol transport results obtained with on-line aerosol measurement devices.

Experiment number		CsI-1	CsI-2	B-1	B-2	B-3
Amount collected on filters determined by ICP-MS [mol]	I	$4.82 \cdot 10^{-5}$	$4.82 \cdot 10^{-5}$	N.A.	$3.22 \cdot 10^{-7}$	$3.00 \cdot 10^{-7}$
	Cs	$5.07 \cdot 10^{-5}$	$5.10 \cdot 10^{-5}$	N.A.	$1.09 \cdot 10^{-6}$	$2.37 \cdot 10^{-8}$
	B	N.A.	N.A.	$5.55 \cdot 10^{-8}$	$5.69 \cdot 10^{-5}$	$5.55 \cdot 10^{-8}$
Amount in the liquid traps determined by ICP-MS [mol]	I	$4.00 \cdot 10^{-7}$	$1.05 \cdot 10^{-7}$	N.A.	$5.80 \cdot 10^{-6}$	$1.47 \cdot 10^{-6}$
	Cs	< LOD	< LOD	N.A.	$2.16 \cdot 10^{-8}$	< LOD
	B	N.A.	N.A.	$6.65 \cdot 10^{-5}$	$4.56 \cdot 10^{-4}$	$1.34 \cdot 10^{-4}$
Number of moles of iodine "I" in molecular iodine (I_2) form [mol]		< LOD	< LOD	N.A.	$4.95 \cdot 10^{-6}$	$2.60 \cdot 10^{-6}$
Number of moles of iodine "I" in water-soluble form (HI or HIO) [mol]		$3.22 \cdot 10^{-8}$	$1.53 \cdot 10^{-8}$	N.A.	$6.06 \cdot 10^{-7}$	$4.91 \cdot 10^{-7}$
Molar ratio measured on the filter	Cs/I	1.05	1.06	N.A.	3.39	0.08
	B/Cs	N.A.	N.A.	N.A.	52.12	2.34
Percentage of gaseous iodine		0.82	0.22	N.A.	94.74	83.07
Percentage of iodine under I_2 form		< LOD	< LOD	N.A.	89.09	84.12
Percentage of gaseous boron		N.A.	N.A.	99.92	88.91	99.96
Initial mass of H_3BO_3 in the crucible [g]		N.A.	N.A.	5.4	5.309	5.383
Mass of residue in the crucible after the test [g]		N.A.	N.A.	2.582	1.912	1.99
Vaporization rate from crucible [mg/min]		N.A.	N.A.	1.6	1.9	1.9
ELPI [1/cm^3]		$9.4 \cdot 10^6$	$9.2 \cdot 10^6$	$8.4 \cdot 10^7$	$1.1 \cdot 10^7$	$2.7 \cdot 10^7$
AMD[8] [nm]		130	160	500	840	420
TEOM [mg/m^3]		5.36	5.94	6.32	13.11	17.55

[7] The PTFE filters were soaked during 24 h into 50 ml of sodium hydroxide solution.

[8] AMD: Aerodynamic Median Diameter. It corresponds to the diameter below which one-half the particles lie and above which one-half the particles lie.

time between the samples was 4 min with pump speed of 11 rpm. The LOD of iodine, caesium and boron were estimated to be $3.0 \cdot 10^{-9}$ mol/l, $1.0 \cdot 10^{-9}$ mol/l and $4.0 \cdot 10^{-8}$ mol/l in sodium hydroxide solution. The measurement uncertainty was ±5.3%. The uncertainty relating to the number of moles was applied to the analysis by ICP-MS. After calculating the contribution of each source of uncertainty (the method of analysis, the dilution factor, the evaluation of the volumes produced by weighing for the tests), the standard uncertainty associated with determining the number of moles was calculated to be 9.5% for iodine and caesium and 10% for boron.

3. Experimental results

Table 2 shows the results obtained from the ICP-MS, UV-spectrometry post analyses and from the on-line measurement devices. The analyses of the stainless steel coupons placed inside the TGT are not presented in the present paper and will be discussed in a future paper with post-analysis study.

3.1. Determination of the size of the particles generated from the stainless steel tube and water droplets

Before studying the transport of particles through the TGT, measurements were performed in order to assess the transport of droplets generated by the steam transiting through the TGT and transport of dust initially present in the stainless tube. A stainless steel tube was heated in the similar conditions of the test. First, only argon was flowing through the TGT. Once temperature of the furnace reached 1023 K, the particle size distribution was monitored online for 30 min. Then, steam was added to the carrier gas and flow rate was adjusted in order to keep same overall flow rate for 30 min. Fig. 4 shows the particle size distribution of the particles passing through the TGT and reaching the ELPI device. The measurements performed in Ar atmosphere revealed the presence of particles coming from the stainless steel TGT. The AMD was 30 nm. The presence of steam in the carrier gas had an influence on the results measured with ELPI, measuring AMD of 50 nm, although in a low amount. TEOM recorded a mass concentration of 2 mg/m^3. After the test, black flakes and cracks were observed in the tube. Knowing the oxidative conditions, a parallel can be done with works on the water vapour inducing breakaway oxidation of stainless steels. According to when exposed to flowing air containing water vapour (5–40 in volume percentage) at temperatures of 970–1170 K, catastrophic breakaway oxidation occurred on the SS304 (Huntz et al., 2007). This could be one explanation of the measured particles by ELPI in the Ar/H_2O atmosphere.

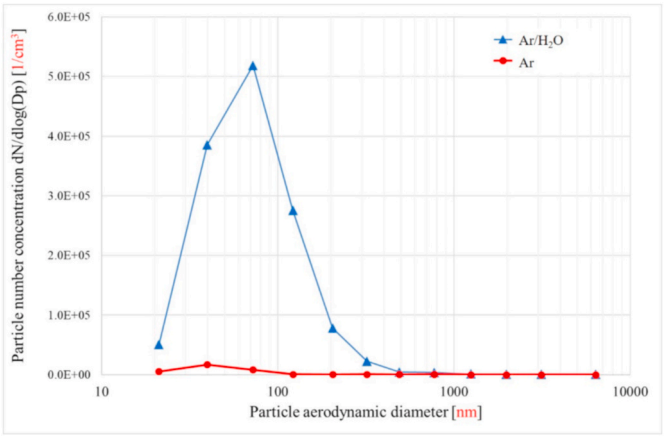

Fig. 4. Number concentration of particles transported through or/and coming from the TGT as a function of the particle aerodynamic diameter (Dp) recorded with ELPI.

3.2. Caesium iodide particle transport through the TGT

The first set of tests was designed to study the transport of caesium iodide aerosols in the TGT. The particle size distribution of the particles passing through the TGT was similar to the one measured directly after the ultrasonic nebulizer looking at the ELPI measurement (Fig. 3). The particles measured with ELPI showed an AMD of about 130 nm (Fig. 3).

The results showed good repeatability between two tests performed with the same conditions. The measurement monitored during sampling 2 (S2) showed a slightly lower value than the measurement conducted during the sampling 1 (S1), which can be can be attributed to the uncertainty of the measurement.

As expected, the Cs/I ratio was close to 1, but with a slight trend to be higher than the unit. That would suggest that the particles collected on filters are mostly made of caesium iodide, and a small fraction is composed by caesium not linked to iodine. The ICP-MS analysis of the trapping solution confirmed this by showing the existence of a small percentage of gaseous iodine (<1%). The UV–Visible spectrometry has a LOD higher[9] than the amount of sampled gaseous iodine (few ppb), it was therefore not possible to determine the percentage of generated molecular iodine.

3.3. Boric acid transport through the TGT

The first test (B-1) was performed in order to assess the behaviour of the gaseous boric acid generated from a crucible.

As the boric acid was generated from a crucible which is placed in a thermal gradient (from 450 K to 1000 K), performing thermodynamic equilibrium calculations was required in order to determine the predominant form of the vaporized boron compound in the whole temperature range and to determine the main compound in gaseous phase at the point where the boron meets the caesium iodide aerosols (at 1020 K).

The thermodynamic equilibrium calculation were performed:

- with FactSage 5.5 and the FACT 5.3 compound database (Bale et al., 2002);
- with NucleaToolbox (Piar, 2016) and the NUCLEA database developed by IRSN (Bakardjieva et al., 2010; Fischer, 2019).

The gaseous and condensed boron species taken into account in the calculation are listed in Table 3 for the two databased utilized.

The calculations performed with NucleaToolbox and the NUCLEA database showed that the vaporization of pure boric acid under Ar/H_2O led mainly to the formation of the trimer of metaboric acid $B_3H_3O_6$(g). The results obtained with FactSage 5.5 displayed $H_3B_3O_3$(g) as the main gaseous species within 400 K and 1000 K (Fig. 5). To our knowledge, the thermodynamic data on boric acid vaporization are rather limited. Nevertheless, one can mention the studies conducted by Stackelberg et al. (1937), Bezzi (1935) and Balasubramanian et al. (2008), using a transpiration method on the H_2O–B_2O_3 system and Knudsen effusion mass spectrometry, from which they deduced the variation of H_3BO_3(g) vapour pressures, the main species, in the temperature interval [315–453 K]. Both thermodynamic databases predict the H_3BO_3(g) species as the predominant one, in agreement with the experimental data, but higher pressures in the Factsage calculations, of one order of magnitude, which seems to be more consistent with the experimental data even if rather dispersed (Balasubramanian et al., 2008; Bezzi, 1935; Pankajavalli et al., 2007; Stackelberg et al., 1937). At higher

[9] The Limit Of Detection of molecular iodine in toluene was measured to be 1 ppm.

[10] The values correspond to the calculated amounts in the last volume.

[11] The percentage of gaseous iodine species (I, HI, HIO, CsI and I_2) in comparison to the sum of iodine species in suspended particles and gas.

Table 3
Gaseous and condensed boron species taken into account in the calculation.

	NUCLEA database	FACT 5.3 compound database
Gaseous species	$B_{10}H_{14}$(g)	$B_{10}H_{14}$(g)
	B_1H_1(g)	BH(g)
	$B_1H_1O_1$(g)1	
	$B_1H_1O_1$(g)2	
	$B_1H_1O_2$(g)	HBO_2(g)
	B_1H_2(g)	BH_2(g)
	$B_1H_2O_1$(g)	HBO(g)
	$B_1H_2O_2$(g)	$B(OH)_2$(g)
	B_1H_3(g)	BH_3(g)
	$B_1H_3O_1$(g)	
	$B_1H_3O_2$(g)	
	$B_1H_3O_3$(g)	H_3BO_3(g)
	$B_2H_4O_4$(g)	$B_2(OH)_4$(g)
	B_2H_6(g)	B_2H_6(g)
	$B_3H_3O_3$(g)	$B_3H_3O_3$(g)
	$B_3H_3O_6$(g)	$(HBO_2)_3$(g)
	B_5H_9(g)	B_5H_9(g)
		$(BO)_2$(g)
		B_2O_3(g)
		BO(g)
		B_2O(g)
		BO_2(g)
		B(g)
		B_2(g)
Condensed species	$B_{10}H_{14}$(c)	$B_{10}H_{14}$(s,l)
	B_5H_9(c)	B_5H_9(l)
	$B_1H_1O_2$(c)	HBO_2(s)
		HBO_2_orthorhombic (s3)
		HBO_2_monoclinic (s2)
	$B_1H_3O_3$(c)	H_3BO_3(s)
	$B_2H_4O_4$(c)	B_2(OH)4(s)
	$B_3H_3O_3$(c)	$B_3H_3O_3$(s)
		B (s,l)
		B_2O_3(s,l)

temperatures up to 1000 K, no experimental data seems to be available. The FactSage calculation in this temperature range shows the presence of both $H_3B_3O_6$(g) and H_3BO_3(g) species more or less in equal amount. Above 1060 K, Meschi et al. (1960) put in evidence the predominance of HBO_2(g) (as predicted by both calculations but at higher temperatures) and the minor quantities of $H_3B_3O_6$(g) and H_3BO_3(g) in the gas phase.

Experimentally, the boron was mostly identified in the liquid trap (>99%), suggesting that the boron was mostly transported as gas from the crucible to the sampling lines (Table 2). The small fraction of boron transported as particles was characterized by a bimodality of the particle size distribution (Fig. 6). The thermodynamic equilibrium calculations showed that the two species H_3BO_3 and $H_3B_3O_6$ are simultaneously present in the temperature range prevailing in the facility. The NucleaToolbox calculates both species to be present in similar amount at 450 K. It is then probable that the bimodality of the particle size distribution is attributed to the presence of those two species.

3.4. Caesium iodide particle transport through the TGT in presence of gaseous boric acid

When the boric acid was added to the caesium iodide particles, the transport of iodine and caesium through the TGT was affected.

By comparing the amount of gaseous iodine released from the vaporization of caesium iodide in similar conditions, the addition of boric acid to caesium iodide distinctly increased the amount of released gaseous iodine (Table 2). The percentage of gaseous iodine, representing less than 1% in the reference case (CsI-1 and CsI-2), reached more than 94% in presence of boric acid (B-2). Increasing the total flow rate in system (B-3) led to decreasing the amount of iodine reaching the sampling line. From 4 l/min to 6 l/min, the amount of gaseous iodine was divided almost by 4.

Molecular iodine in toluene forms a complex which exhibits two absorption peaks centred at 306 nm and 498 nm (Benesi and Hildebrand, 1949). These characteristic peaks were measured in all toluene solutions (Table 2). Molecular iodine was the main gaseous species; representing 89% of the total gaseous iodine in test B-2. This percentage remained high for the test B-3 (84%).

The vaporization rate has been calculated from the loss of mass of boric acid in the crucible after the test and the duration of the test (Table 2). It showed a higher vaporization rate in presence of caesium iodide particles (1.9 mg/min by comparison to 1.6 mg/min for the vaporization of boric acid). As it was mentioned in paragraph 4.2, the amount of boric acid in gaseous phase is increased by the presence of water. As the particles of caesium iodide where introduced from a solution of caesium iodide, it is suspected that the droplets were dried

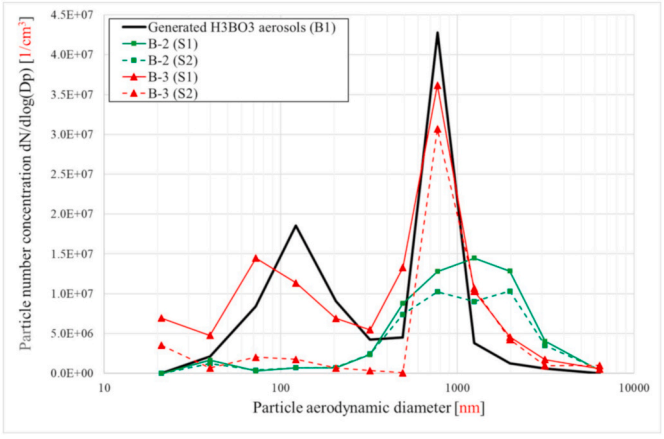

Fig. 6. Number concentration of particles obtained from the vaporization of boric acid in black and particles transported through the TGT following interaction between boric acid and caesium iodide as a function of the particle aerodynamic diameter (Dp) recorded with ELPI.

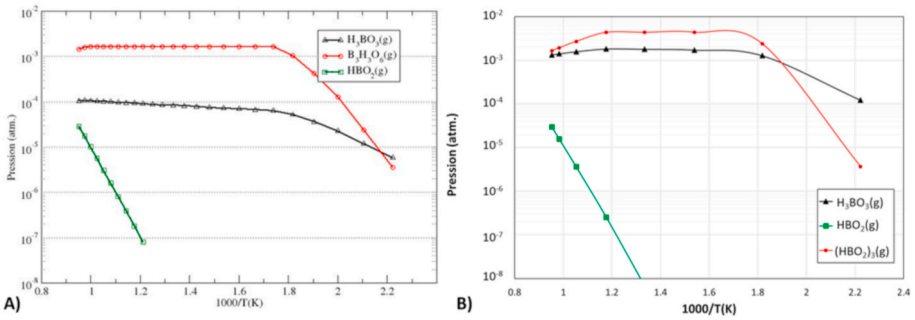

Fig. 5. Main boron gaseous species formed when heating boric acid from 450 K to 1050 K in Ar/H_2O (80/20 vol%) calculated in chemical equilibrium with A) NucleaToolbox and the NUCLEA database developed by IRSN and B) Thermfact and GTT-Technologies FactSage 5.5.

while entering in the furnace, leading to an increase of the total amount of steam in gaseous phase. This would explain the higher stability of boric acid in gaseous phase, then its higher vaporization rate.

On the filters, lower amounts of iodine as particle were collected when boron was present (Table 2) than during the reference case (CsI-1 and CsI-2). The amount of caesium was also decreased on the filter, suggesting that a fraction of the caesium from caesium iodide particles was retained in the TGT. The proportion of boron as particles increased from the test B-1 to the test B-2. This would imply that boron has reacted with caesium iodide forming condensable species collected on the filter. The increase of the total flow rate (B-3) showed similar percentage of gaseous boron as it was measured in the reference test B-1. This would signify that less boron has reacted with the caesium iodide forming condensable species. The Cs/I molar ratio on the filter became higher than 1 in B-2, suggesting the presence of caesium compound other than caesium iodide. The B/Cs molar ratio revealed a higher amount of boron than caesium on the filter.

The TEOM measurements showed higher mass concentration of particles than the particles collected during the vaporization of boric acid or the transport of caesium iodide particles. The particle number concentration was the highest for the vaporization of boric acid test B-1 (Table 2) and the lowest for the vaporization of caesium iodide (CsI-1 and CsI-2). The ELPI measurement showed bimodal distribution (Fig. 6).

4. Analysis with the SOPHAEROS module of ASTEC code

The ASTEC (Accident Source Term Evaluation Code) was jointly developed until 2015 by the French "Institut de Radioprotection et de Sûreté Nucléaire" (IRSN) and the German "Gesellschaft für Anlagen und Reaktorsicherheit mbH" (GRS), and developed now only by IRSN, for severe accident analysis for which it simulates the overall nuclear power plant response. The ASTEC/SOPHAEROS module (version v2.1_1_4 described in detail in Cousin et al. (2008) computes chemistry and transport of the fission products in the Pressurized Water Reactor (PWR) RCS during a severe accident. The geometry is represented by a sequence of 1D control volumes assembled by junctions. The modelling is based on a set of mass balance equations where the main phenomena governing the vapour and aerosol phases are represented. Phenomena taken into account for vapours and aerosols are listed below:

a) Vapour-phase phenomena
   - Gas equilibrium chemistry for up to 800 species (Kaye et al., 2010).
   - Chemisorption of vapours on walls.
   - Homogeneous and heterogeneous nucleation.
   - Condensation/revaporization on/from aerosols and walls.

b) Aerosol phenomena
   - Agglomeration: gravitational, Brownian and turbulent diffusion.
   - Deposition mechanisms: Brownian diffusion, turbulent diffusion, eddy impaction, sedimentation, thermophoresis, diffusiophoresis, impaction in bends.
   - Remobilisation of deposits: revaporization from deposited aerosols and mechanical resuspension.

A sectional approach is adopted to model the aerosols distribution. The same species composition is considered in all the aerosol size classes.

4.1. Modelling the experimental facility and definition of the boundary conditions

The most important thermal-hydraulic parameters affecting the fission products transport are the gas and wall temperatures, the pressure, flow rate and the gas composition. In the case of the present tests, the pressure was constant and set at atmospheric pressure. Preliminary measurements with a moving thermocouple in the TGT allowed defining the thermal profile of the gas in the axial direction. In addition, five thermocouples were placed outside the stainless steel tube walls at a known abscissa (see Fig. 1) and recorded the outside wall temperature during the tests.

The geometric domain was limited to the zone located between the highest temperature point in the TGT (abscissa = 0.2 m) and the outlet of the tube (abscissa = 0.8 m). The TGT was modelled as the succession of 40 control volumes. Thermal fluid and outside wall profiles from thermal-hydraulic qualification were used to create the axial mesh of the tube. Input data were deduced from the tests and from qualification tests (mass flow rate of CsI, mass flow rate of H_3BO_3, mass flow rate of steam and argon). As the inner wall temperature was not measured experimentally, it was first approximated from CFD analysis tool, CHASER, developed by JAEA based on the commercial ANSYS-FLUENT (Miwa et al., 2019a; Miyahara et al., 2017). Fig. 2 presents the thermal profile with the experimentally measured temperatures and the temperatures approximated by the CFD analysis for the studied atmosphere composition and flow rate.

The chemical elements were injected into the first volume with their respective experimental mass flow rates. Standard models and recommended parameters were used for the different physical and chemical phenomena to be representative of plant simulations. The injection form of the caesium iodide was determined as aerosol, as is the case experimentally. The geometric median radius of the first and second distribution was settled from the ELPI measurements (Fig. 3).

4.2. Analysis of the caesium iodide transport

The first analysis was performed using the temperature of the flow calculated at the centre of the tube. Table 4 presents the calculated results. Table 5 summarizes the comparison between experimental results and results obtained with SOPHAEROS (obtained using the calculated bulk temperatures).

The caesium iodide particles were mostly transported as particles through the TGT. A slight decomposition happened at the highest temperature, leading to the formation of gaseous caesium hydroxide and iodine, but with the decrease of the temperature, the caesium iodide was reformed. At 1015 K, the gaseous species already started to condense, with a peak of CsI/Cs_2I_2 condensation around 1000 K. The amount of CsI in gaseous phase decreased. The condensation peak was also associated with the increase of the aerosols in suspension and deposited aerosols (CsI and Cs_2I_2). The evolution of the condensed species on the walls was initially fast, and then it tended to decrease by consumption of the gas phase and by condensation on the aerosols. For temperatures lower than 710 K, no more gaseous species existed in gaseous phase. Hence, all the iodine and caesium were either condensed or in aerosol form. The experimental results showed a quite similar tendency, with the measurement of less than 1% of gaseous iodine at the outlet of the TGT (Table 2). The AMD of the suspended particles was calculated to be 455 nm at 400 K, which was larger than the experimentally measured values by ELPI (130 nm, see Table 3) and the average number concentration was much lower than the experimental one. Considering the temperature differences between the gas and wall, the main aerosol deposition mechanism was thermophoresis.

The second analysis was performed using the temperature of the gas calculated considering the bulk temperature. In this configuration, the observed trends were similar to those for the analysis performed with temperature at the centre of the TGT. However, as the difference between the wall temperature and the temperature of the flow was smaller, consequences were noticed, notably on the condensation and formation of aerosols. The action of the thermal gradient between the gas temperature and the wall temperature has a great influence on the retention of the species (gas and particles). Nevertheless, computations in both cases led to a high percentage of particles in suspension at 400 K (>99%), which was in agreement with the experimental measurements. The AMD of the suspended particles was calculated to be 214 nm at 400 K, which is closer to the experimentally measured values by ELPI than

Table 4
Transported amounts[10] of iodine, caesium and boron in the tests, calculated with the version v2.1_1_6 of the ASTEC/SOPHAEROS module.

Experiment number		Gas centre				Gas bulk			
		CsI-1	B-1	B-2	B-3	CsI-1	B-1	B-2	B-3
Amount in suspended aerosol form calculated at 411 K [mol]	I	$1.3{\cdot}10^{-7}$	N.A.	$2.3{\cdot}10^{-7}$	$1.3{\cdot}10^{-7}$	$1.0{\cdot}10^{-6}$	N.A.	$1.0{\cdot}10^{-6}$	$6.5{\cdot}10^{-7}$
	Cs	$1.3{\cdot}10^{-7}$	N.A.	$2.3{\cdot}10^{-7}$	$1.3{\cdot}10^{-7}$	$1.0{\cdot}10^{-6}$	N.A.	$1.0{\cdot}10^{-6}$	$6.5{\cdot}10^{-7}$
	B	N.A.	$2.6{\cdot}10^{-11}$	$1.9{\cdot}10^{-8}$	$9.6{\cdot}10^{-9}$	N.A.	$1.1{\cdot}10^{-9}$	$4.5{\cdot}10^{-6}$	$3.3{\cdot}10^{-6}$
Amount in gaseous form calculated at 411 K [mol]	I	$9.1{\cdot}10^{-17}$	N.A.	$1.4{\cdot}10^{-9}$	$7.7{\cdot}10^{-10}$	$6.2{\cdot}10^{-15}$	N.A.	$4.1{\cdot}10^{-10}$	$2.3{\cdot}10^{-10}$
	Cs	$6.1{\cdot}10^{-13}$	N.A.	$1.5{\cdot}10^{-16}$	$9.1{\cdot}10^{-17}$	$7.7{\cdot}10^{-19}$	N.A.	$5.7{\cdot}10^{-16}$	$3.9{\cdot}10^{-16}$
	B	N.A.	$2.1{\cdot}10^{-8}$	$2.8{\cdot}10^{-8}$	$1.5{\cdot}10^{-8}$	N.A.	$7.9{\cdot}10^{-7}$	$1.1{\cdot}10^{-7}$	$1.1{\cdot}10^{-7}$
Number of moles of iodine "I" in molecular iodine (I_2) form [mol]		$8.8{\cdot}10^{-14}$	N.A.	$2.1{\cdot}10^{-10}$	$1.1{\cdot}10^{-10}$	$7.7{\cdot}10^{-32}$	N.A.	$6.2{\cdot}10^{-11}$	$3.4{\cdot}10^{-11}$
Number of moles of iodine "I" in water-soluble form (HI, I or HIO) [mol]		$5.2{\cdot}10^{-13}$	N.A.	$1.2{\cdot}10^{-9}$	$6.6{\cdot}10^{-10}$	$2.1{\cdot}10^{-23}$	N.A.	$3.5{\cdot}10^{-10}$	$1.9{\cdot}10^{-10}$
Molar ratio determined from aerosol in suspension	Cs/I	1.00	N.A.	1.00	1	1.00	N.A.	1.00	1.00
	B/Cs	N.A.	N.A.	0.09	0.07	N.A.	N.A.	4.49	5.15
Percentage of gaseous iodine[11]		0	N.A.	0.61	0.59	0	N.A.	0.04	0.04
Percentage of iodine under I_2 form		0	N.A.	14.9	14.9	0	N.A.	15.02	14.99
Percentage of gaseous boron		N.A.	54.59	58.99	60.92	N.A.	99.86	2.45	3.16
Average number concentration of suspended particles [1/cm^3]		$8.6{\cdot}10^{4}$	$1.9{\cdot}10^{2}$	$1.9{\cdot}10^{5}$	$1.1{\cdot}10^{5}$	$6.9{\cdot}10^{6}$	$6.2{\cdot}10^{3}$	$7.46{\cdot}10^{6}$	$1.1{\cdot}10^{7}$
AMD [nm]		455	2471	455	455	214	13,415	259	178
Suspended aerosol main species		Cs_2I_2	$B_3H_3O_6$	Cs_2I_2 $B_3H_3O_6$	Cs_2I_2 $B_3H_3O_6$	Cs_2I_2	$B_3H_3O_6$	Cs_2I_2 $B_3H_3O_6$	Cs_2I_2 $B_3H_3O_6$

Table 5
Summarizing comparative table between data calculated with the version v2.1_1_6 of the ASTEC/SOPHAEROS module (obtained using the calculated bulk temperatures) and experimental data.

Experiment number		CsI-1		B-1		B-2		B-3	
Source of data (SOPH:SOPHAEROS; EXP: experiment)		SOPH.	EXP.	SOPH.	EXP.	SOPH.	EXP.	SOPH.	EXP.
Amount in suspended aerosol form calculated at 411 K [mol]	I	$1.0{\cdot}10^{-6}$	$4.82{\cdot}10^{-5}$	N.A.	N.A.	$1.0{\cdot}10^{-6}$	$3.22{\cdot}10^{-7}$	$6.5{\cdot}10^{-7}$	$3.00{\cdot}10^{-7}$
	Cs	$1.0{\cdot}10^{-6}$	$5.07{\cdot}10^{-5}$	N.A.	N.A.	$1.0{\cdot}10^{-6}$	$1.09{\cdot}10^{-6}$	$6.5{\cdot}10^{-7}$	$2.37{\cdot}10^{-8}$
	B	N.A.	N.A.	$1.1{\cdot}10^{-9}$	$5.55{\cdot}10^{-8}$	$4.5{\cdot}10^{-6}$	$5.69{\cdot}10^{-5}$	$3.3{\cdot}10^{-6}$	$5.55{\cdot}10^{-8}$
Amount in gaseous form calculated at 411 K [mol]	I	$6.2{\cdot}10^{-15}$	$4.00{\cdot}10^{-7}$	N.A.	N.A.	$4.1{\cdot}10^{-10}$	$5.80{\cdot}10^{-6}$	$2.3{\cdot}10^{-10}$	$1.47{\cdot}10^{-6}$
	Cs	$7.7{\cdot}10^{-19}$	< LOD	N.A.	N.A.	$5.7{\cdot}10^{-16}$	$2.16{\cdot}10^{-8}$	$3.9{\cdot}10^{-16}$	< LOD
	B	N.A.	N.A.	$7.9{\cdot}10^{-7}$	$6.65{\cdot}10^{-5}$	$1.1{\cdot}10^{-7}$	$4.56{\cdot}10^{-4}$	$1.1{\cdot}10^{-7}$	$1.34{\cdot}10^{-4}$
Number of moles of iodine "I" in molecular iodine (I_2) form [mol]		$7.7{\cdot}10^{-32}$	< LOD	N.A.	N.A.	$6.2{\cdot}10^{-11}$	$4.95{\cdot}10^{-6}$	$3.4{\cdot}10^{-11}$	$2.60{\cdot}10^{-6}$
Number of moles of iodine "I" in water-soluble form (HI or HIO) [mol]		$2.1{\cdot}10^{-23}$	$3.22{\cdot}10^{-8}$	N.A.	N.A.	$3.5{\cdot}10^{-10}$	$6.06{\cdot}10^{-7}$	$1.9{\cdot}10^{-10}$	$4.91{\cdot}10^{-7}$
Molar ratio determined from aerosol in suspension	Cs/I	1.00	1.05	N.A.	N.A.	1.00	3.39	1.00	0.08
	B/Cs	N.A.	N.A.	N.A.	N.A.	4.49	52.12	5.15	2.34
Percentage of gaseous iodine		0	0.82	N.A.	N.A.	0.04	94.74	0.04	83.07
Percentage of iodine under I_2 form		0	< LOD	N.A.	N.A.	15.02	89.09	14.99	84.12
Percentage of gaseous boron		N.A.	N.A.	99.86	99.92	2.45	88.91	3.16	99.96
Average number concentration of suspended particles [1/cm^3]		$6.9{\cdot}10^{6}$	$9.4{\cdot}10^{6}$	$6.2{\cdot}10^{3}$	$8.4{\cdot}10^{7}$	$7.46{\cdot}10^{6}$	$1.1{\cdot}10^{7}$	$1.1{\cdot}10^{7}$	$2.7{\cdot}10^{7}$
AMD [nm]		214	130	2470	500	259	840	178	420

the one defined from calculations with gas centre. In addition, the average number concentration of the suspended particles was in the same order of magnitude as the experimentally measured one.

4.3. Analysis of the boric acid transport

The results of the analysis performed with bulk and centre flow temperatures showed that boron was entirely transported through the TGT as gas, mostly as metaboric acid trimer, $(HBO_2)_3$. The condensation of metaboric acid trimer started at the point where the flow temperature was about 810 K and the wall temperature was about 660 K. Experimentally particles were measured, it was then suspected that they come from condensation of gaseous boric acid on already existing particles (heterogeneous nucleation). The dust particles could be due to the oxidation of the stainless tube by the steam. Consequently, iron oxide particles (Fe_2O_3) were initially injected into the computation. The size distribution of the iron oxide particles was chosen by default as recommended in the code (lognormal distribution, with an initial radius of 0.5 μm and a standard of deviation of 1.5). The mass injected was fixed to 10^{-13} kg/s at t = 0 and at the end of the calculation 0.

The first analysis was performed using the temperature of the flow calculated at the centre of the tube. In gaseous phase, the trimer of metaboric acid $(HBO_2)_3$ predominated. Condensation of this species started at 900 K. Suspended particles appeared around 540 K. At the outlet of the facility, the boron in gaseous phase represented 54.59% of the boron total (gas + suspended particles).

The analysis performed using the temperature of the flow calculated at the bulk, showed results closer to the experimental results (Table 3). The boron in gaseous phase represented 99.86%, against 99.92% calculated from the experimental results. However, the size distribution did not display similar trend.

4.4. Analysis of the caesium iodide transport in presence of boric acid

For the tests B-2 and B-3, the main gaseous species were the same as the ones calculated for B-1. The trimer of metaboric acid was the majority species in gaseous phase, with orthoboric acid (H_3BO_3) and caesium iodide. While the condensation of caesium iodide and its dimer started at high temperature (from 925 K), condensation of the trimer of metaboric acid showed a condensation peak at 900 K. The dimer of caesium iodide was the main species of the suspended particles calculated in the TGT, the trimer of metaboric acid being present in 100 times lower amount. The results of the SOPHAEROS calculations, both for gas bulk and gas centre, did not account for the experimental results. The percentage of gaseous iodine hardly reached 1% (Table 3) and the B/Cs and Cs/I molar ratios on the filters were different from the measured

values.

The vaporization of higher amount of initial boric acid (B-3) resulted in increasing the amount of boron on the filter but no significant difference on the generated amount of gaseous iodine was induced. The results of the SOPHAEROS analysis would suggest that there is no interaction between the gaseous boric acid and the caesium iodide as particles, in the studied conditions.

5. Discussion and conclusions

In the framework of the Academy of Finland SA-AERIS project, small-scale tests were performed to understand better the transport and chemistry of caesium iodide as particles and gaseous boric acid in a thermal gradient tube. The objectives were to study the interaction between caesium iodide as particles and gaseous boric acid and to compare the experimental results with results obtained from SOPHAEROS analysis.

Despite the laminar flowrate, not representative of realistic severe accident conditions, the thermal-hydraulic conditions settled for the tests presented two main important parameters for the study, i.e. the experimental residence time comprised between 2 s and 3.3 s and temperature profile from 1023 K to 423 K.

In the studied conditions, the introduced caesium iodide particles transited through the TGT as particles and only a small fraction of particles decomposed into gaseous iodine (<3%). The deposition of the particles in the TGT was underlined by comparing the amount of particles measured directly after the aerosol generator and the amount of particles passing through the TGT. As previously observed in (Dehbi et al., 2016), the steam condensation could significantly enhance aerosol deposition. In the present case, the temperatures of the TGT walls were lower than the carrier gas temperature, especially in the region 0.2–0.45 m. The ASTEC/SOPHAEROS module predicted that the caesium iodide particles transited through the TGT mostly as particles, as observed experimentally. The measurement of a small fraction of gaseous iodine (less than 1%) was not predicted by the ASTEC/SOPHAEROS calculation. This slight decomposition of caesium iodide could be explained by the results of the interaction of condensed steam on the surface of the particles, caesium iodide being hygroscopic and soluble in water. The calculated suspended particles at 400 K showed larger diameter than the experimentally measured ones. However, the number concentration was in agreement with the experimental measurements. That might be explained by the over prediction either of steam condensation onto the caesium iodide particles or coagulation of the submicron particles.

The experimental results, regarding the transport of boric acid through the TGT, suggest that boron was mostly transported in the gaseous phase. A small fraction of boron was also identified as particles (<0.1% of the total amount of boron measured in the sampling lines). The experimental results are consistent to those obtained from the transport of boric acid through a TGT (from 1820 K to 400 K), although performed with much higher proportion of steam in the carrier gas (Ar/H_2O (20/80 vol%)) (Gouëllo, 2012). To the contrary, results observed by Miwa et al. in the TeRRa facility (Miwa et al., 2019b), after vaporizing boric trioxide powder at 1150 K and studying its transport through at TGT (from 1000 K to 400 K) in Ar/H_2O (80/20 vol%) atmosphere, showed highest amount of boron as particles. Most of the injected boron had nucleated and condensed. The TGT zone in the TeRRa facility is defined from 1000 K to 400 K by a stainless steel tube type 304 l (diameter 0.4 m, length 0.8 m) and is heated externally. In EXSI-AERIS, the TGT is defined from 1000 K to 400 K by a stainless steel tube type AISI 304 (diameter 0.25 m, length 0.6 m) and is only insulated. Most importantly, in the EXSI-AERIS facility, a flow rate of 4 l/min was investigated while in the TeRRa facility; a flow rate of 2.4 l/min was imposed. The measurement of particles during the vaporization of boric acid in EXSI-AERIS was attributed to the condensation of boric acid onto existing dust particles. The SOPHAEROS analysis showed results quite similar to the experimental results, by transporting boric acid mostly as gas through the TGT.

When boric acid was vaporized when the caesium iodide particles were introduced inside the facility, gaseous iodine was measured in the sampling lines (>80% of total sampled iodine). This would evidence a reaction between the boric acid and the caesium iodide. Based on Bowsher's equations used to describe the reaction between the two compounds in condensed phase (Bowsher and Nichols, 1985):

$$CsI(c) + H_3BO_3(g) \rightarrow CsBO_2(c) + HI(g) + H_2O(g)$$

$$2HI(g) \leftrightarrow I_{2(g)} + 2H_2(g)$$

In addition, the rate of reaction seems to be lower when the flow rate inside the facility was increased; based on the measurement of lower amount of gaseous iodine at the outlet of the facility. The higher gas velocity and lower residence time would explain the lower rate of formation of gaseous iodine. As the temperature difference between the gas and the wall inside the TGT was higher for a 6-l/min flow rate than for a 4-l/min flow rate, it would be possible that the condensation of boric acid onto particles take place in competition with the condensation onto cooler wall surface.

The results of SOPHAEROS analysis did not manifest such interaction between the particles and the gas, as the models are not yet included in the code. In the code, only the congruent condensation/revaporization on/from aerosol are modelled.

This study presented preliminary results on the potential interaction between vapours of boric acid and caesium iodide particles. First results have shown that the reaction can be significant under specific conditions and could affect the transport of iodine in a TGT. In order to keep assessing the potential for vapour boric acid to react with caesium iodide particles, more conditions should be investigated, such as carrier gas composition and reactant concentrations, and the experiments should be repeated. The reaction of boric acid vapours with caesium iodide aerosols in static system should also be examined to provide complementary data. The static system studies involve heating samples of caesium iodide particles deposited on stainless steel coupons in different boric acid-steam-argon atmospheres, and are currently subject of a work programme at JAEA.

CHASER has turned out to be a great tool for assessing the temperatures inside the TGT based on the limited experimental data. Using the calculated bulk temperatures proved to be better for the simulation of the chemical reactions and particles behaviour than using the centre temperatures.

The assessment of the main boron species generated from the vaporization of boric acid in Ar/H_2O atmosphere by NucleaToolbox ($B_3H_3O_6$(g)) and by FactSage 5.5 ($B_3H_3O_6$(g) and H_3BO_3(g)) have shown differences. It highlighted the important role of a reliable and validated database.

Overall, the ASTEC fission products models allowed performing the evaluation of the experimentally observed results for the analysis of the transport of pure compounds. However, heterogeneous reaction between gaseous boric acid and caesium iodide particles was not reproduced, as the phenomena are not yet taken into account. More work is in progress in order to further investigate this interaction and to determine the need to develop the database and models.

Declaration of competing interest

The authors declare that they have no known competing financial interests or personal relationships that could have appeared to influence the work reported in this paper.

Acknowledgments

This work was supported by the Academy of Finland under Grant no. 294995.

References

Bakardjieva, S., Barrachin, M., Bechta, S., Bottomley, D., Brissoneau, L., Cheynet, B., Fischer, E., Journeau, C., Kiselova, M., Mezentseva, L., Piluso, P., Wiss, T., 2010. Improvement of the European thermodynamic database NUCLEA. Prog. Nucl. Energy 52, 84–96. https://doi.org/10.1016/j.pnucene.2009.09.014.

Balasubramanian, R., Lakshmi Narasimhan, T.S., Viswanathan, R., Nalini, S., 2008. Investigation of the vaporization of boric acid by transpiration thermogravimetry and knudsen effusion mass spectrometry. J. Phys. Chem. B 112, 13873–13884.

Bale, C.W., Chartrand, P., Degterov, S.A., Eriksson, G., Hack, K., Ben Mahfoud, R., Melançon, J., Pelton, A.D., Petersen, S., 2002. FactSage thermochemical software and databases. Calphad 26, 189–228. https://doi.org/10.1016/S0364-5916(02)00035-4.

Barrachin, M., de Luze, O., Haste, T., Repetto, G., 2013. Late phase fuel degradation in the Phébus FP tests. Ann. Nucl. Energy. https://doi.org/10.1016/j.anucene.2013.03.041.

Benesi, H.A., Hildebrand, J.H., 1949. A spectrophotometric investigation of the interaction of iodine with aromatic hydrocarbons. J. Am. Chem. Soc. 71, 2703–2707.

Bezzi, S., 1935. Unknow title. Gazz. Chim. Ital. 65, 766–772.

Bowsher, B.R., Nichols, A.L., 1985. High Temperature Studies of Simulant Fission-Products: Part. IV, Interaction of Caesium Iodide with Boric Acid over the Temperature Range 400 to 1000°C. United Kingdom Atomic Energy Authority (UKAEA), Winfrith (United Kingdom).

Bowsher, B.R., Bruce, D.M., Dickinson, S., 1985. The Interaction of Caesium Iodide with Boric Acid in the Temperature Range 100 to 1000°C, pp. 275–289.

Bowsher, B.R., Dickinson, S., Atomic Energy Establishment, W., 1986. The Interaction of Caesium Iodide with Boric Acid: Vapour Phase and Vapour-Condensed Phase Reactions. United Kingdom Atomic Energy Establishment, Report AEEW-R-2102, Winfrith, United Kingdom https://doi.org/ISBN:961-6207-25-3.

Cantrel, L., Krausmann, E., 2003. Reaction kinetics of a fission-product mixture in a steam-hydrogen carrier gas in the Phébus primary circuit. Nucl. Technol. 144, 1–15. https://doi.org/10.13182/NT03-A3425.

Cantrel, L., Louis, F., Cousin, F., 2013. Advances in mechanistic understanding of iodine behaviour in PHEBUS-FP tests with the help of ab initio calculations. Ann. Nucl. Energy 61, 170–178. https://doi.org/10.1016/j.anucene.2013.02.034.

Cousin, F., Dieschbourg, K., Jacq, F., 2008. New capabilities of simulating fission product transport in circuits with ASTEC/SOPHAEROS v. 1.3. Nucl. Eng. Des. 238, 2430–2438. https://doi.org/10.1016/j.nucengdes.2008.03.018.

Cousin, F., Cantrel, L., Séropian, C., Chevalier-Jabet, K., 2011. Source term computation with ASTEC code. In: International Congress on the Advances in Nuclear Power Plants (ICAPP). Societe Francaise d'Energie Nucleaire, Nice (France), pp. 1103–1112.

Dehbi, A., Suckow, D., Lind, T., Guentay, S., Danner, S., Mukin, R., 2016. Key findings from the artist project on aerosol retention in a dry steam generator. Nucl. Eng. Technol. 48, 870–880. https://doi.org/10.1016/j.net.2016.06.001.

Di Giuli, M., Haste, T., Biehler, R., Bosland, L., Herranz, L.E., Fontanet, J., Beuzet, E., Torkhani, M., Davidovich, N., Klein-Heßling, W., Weber, S., Dickinson, S., Horváth, G., Kruse, P., Koch, M., Paci, S., Weber, S.J., Salay, M., Bujan, A., Ivanov, I., Kalychev, P., Kim, S.B., Morandi, S., del Corno, A., Kotouč, M., Dienstbier, J., Kim, H.-C., 2016. SARNET benchmark on Phébus FPT3 integral experiment on core degradation and fission product behaviour. Ann. Nucl. Energy 93, 65–82. https://doi.org/10.1016/J.ANUCENE.2016.01.046.

Fischer, E., 2019. NUCLEA Thermodynamic Database for Corium Applications. Institut de Radioprotection et Sûreté Nucléaire IRSN Technical Report.

Fisher, Thermo, 2009. Continuous particulate TEOM monitor, Series 1400ab:Product detail [WWW Document]. Waltham, Mass. Thermo Fish. Sci. Inc. URL. https://www.thermofisher.com/document-connect/document-connect.html?url=https%3A%2F%2Fassets.thermofisher.com%2FTFS-Assets%2FLSG%2FSpecification-Sheets%2FD19391~.pdf&title=U3BlY2lmaWNhdGlvbiBTaGVldDogQW1iaWVudCBQYXJ0aWN1bGF0ZSBNb25pdG9yLCBURU9NIDE0MDBhYg=.

Girault, N., Payot, F., 2013. Insights into iodine behaviour and speciation in the Phébus primary circuit. Ann. Nucl. Energy 61, 143–156. https://doi.org/10.1016/j.anucene.2013.03.038.

Gouëllo, M., 2012. Chimie de l'Iode et Composition des Aérosols dans le Circuit Primaire d'un Réacteur Nucléaire. Université de Grenoble, Grenoble.

Gouëllo, M., Lacoue-Nègre, M., Mutelle, H., Sobanska, S., Cousin, F., Blanquet, E., 2012. Chemistry of iodine and aerosol composition in the primary circuit of a nuclear power plant. In: 21st International Conference Nuclear Energy for Europe. Nuclear Society of Slovenia, Ljubljana, Slovenia, pp. 509.1–509.8.

Gouëllo, M., Hokkinen, J., Kärkelä, T., Auvinen, A., 2018. A scoping study of chemical behaviour of caesium iodide in presence of boron in condensed phase (650 °C and 400 °C) under primary circuit conditions. Nucl. Technol. 203, 66–84. https://doi.org/10.1080/00295450.2018.1429111.

Gouëllo, M., Hokkinen, J., Kärkelä, T., 2020. Advances in the understanding of molybdenum effect on iodine and caesium reactivity in condensed phase in the primary circuit in nuclear severe accident conditions. Nucl. Eng. Technol. 52, 1638–1649. https://doi.org/10.1016/j.net.2020.01.029.

Haste, T., Clément, B., Biard, B., Manenc, C., Payot, F., March, P., Simondi-Teisseire, B., Zeyen, R., 2011. Phebus FPT3: overview of main results concerning core degradation and fission product behaviour. In: International Congress on the Advances in Nuclear Power Plants (ICAPP). Societe Francaise d'Energie Nucleaire, Nice (France), pp. 1093–1102.

Haste, T., Payot, F., Dominguez, C., March, P., Simondi-Teisseire, B., Steinbrück, M., 2012. Study of boron behaviour in the primary circuit of water reactors under severe accident conditions: a comparison of phebus FPT3 results with other recent integral and separate-effects data. In: Nucl. Eng. Des., Selected and Expanded Papers from International Conference Nuclear Energy for New Europe 2010, Portoro?, Slovenia, vol. 246, pp. 147–156. https://doi.org/10.1016/j.nucengdes.2011.08.031. September 6-9, 2010.

Haste, T., Payot, F., Bottomley, P.D.W., 2013. Transport and deposition in the Phébus FP circuit. Ann. Nucl. Energy 61, 102–121.

Haste, T., Payot, F., Manenc, C., Clément, B., March, P., Simondi-Teisseire, B., Zeyen, R., 2013. Phébus FPT3: overview of main results concerning the behaviour of fission products and structural materials in the containment. Nucl. Eng. Des. 261, 333–345. https://doi.org/10.1016/j.nucengdes.2012.09.034.

Hinds, W.C., 1999. Aerosol Technology: Properties, Behavior, and Measurement of Airborne Particles. In: Wiley, John (Ed.). Wiley-interscience, New York/Chichester/Weinheim/Brisbane/Singapore/Toronto.

Honaiser, E.H.R., 2003. Development of Fission-Products Transport Model in Severe-Accident Scenarios for SCDAP/RELAP5. University of Florida.

Huntz, A.M., Reckmann, A., Haut, C., Sévérac, C., Herbst, M., Resende, F.C.T., Sabioni, A.C.S., 2007. Oxidation of AISI 304 and AISI 439 stainless steels. Mater. Sci. Eng. A 447, 266–276. https://doi.org/10.1016/j.msea.2006.10.022.

Kärkelä, T., Kajan, I., Tapper, U., Auvinen, A., Ekberg, C., 2017. Ruthenium transport in an RCS with airborne CsI. Prog. Nucl. Energy 99, 38–48. https://doi.org/10.1016/j.pnucene.2017.04.019.

Kaye, M.H., Kissane, M.P., Mason, P., 2010. Progress in chemistry modelling for vapour and aerosol transport analyses. Int. J. Mater. Res. 101, 1571–1578. https://doi.org/10.3139/146.110440.

Meschi, D.J., Chupka, W.A., Berkowitz, J., 1960. Heterogeneous reactions studied by mass spectrometry. I. Reaction of B2O3(s) with H2O(g). J. Chem. Phys. 33, 530–533. https://doi.org/10.1063/1.1731179.

Miwa, S., Yamashita, S., Osaka, M., 2016. Prediction of the effects of boron release kinetics on the vapor species of cesium and iodine fission products. Prog. Nucl. Energy 92, 254–259. https://doi.org/10.1016/J.PNUCENE.2016.02.023.

Miwa, S., Miyahara, N., Nakajima, K., Nishioka, S., Suzuki, E., Horiguchi, N., Liu, J., Miradji, F., Imoto, J., Mohamad, A., Takase, G., Karasawa, H., Osaka, M., 2019a. Development of fission product chemsitry database ECUME for the LWR severe accident. In: 27th International Conference on Nuclear Engineering, pp. 1–8. Ibaraki (Japan).

Miwa, S., Takase, G., Imoto, J., Nishioka, S., Miyahara, N., Osaka, M., 2019b. Boron chemistry during transportation in the high temperature region of a boiling water reactor under severe accident conditions. J. Nucl. Sci. Technol. 1–10. https://doi.org/10.1080/00223131.2019.1671913.

Miyahara, N., Miwa, S., Nakajima, K., Osaka, M., 2017. Development of experimental and analytical technologies for fission product chemistry under LWR severe accident condition. In: Water Reactor Fuel Performance Meeting. Jeju Island, (Korea), pp. 1–9.

Miyahara, N., Miwa, S., Gouëllo, M., Imoto, J., Horiguchi, N., Sato, I., Osaka, M., 2020. Experimental study on transport behavior of cesium iodide in the reactor coolant system under LWR severe accident conditions [WWW document]. J. Nucl. Sci. Technol. https://doi.org/10.1080/00223131.2020.1782281.

Nowack, H., Chatelard, P., Chailan, L., Hermsmeyer, S., Sanchez, V., Herranz, L., 2018. Cesam – code for European severe accident management, EURATOM project on ASTEC improvement. Ann. Nucl. Energy 116, 128–136. https://doi.org/10.1016/j.anucene.2018.02.021.

Pankajavalli, R., Anthonysamy, S., Ananthasivan, K., Vasudeva Rao, P.R., 2007. Vapour pressure and standard enthalpy of sublimation of H3BO3. J. Nucl. Mater. 362, 128–131. https://doi.org/10.1016/j.jnucmat.2006.12.025.

Piar, B., 2016. NucleaToolbox 1.3 User's Manual. Institut de Radioprotection et Sûreté Nucléaire IRSN Technical Report.

Sehgal, B.R., 2001. Accomplishments and challenges of the severe accident Research. Nucl. Eng. Des. 210, 79–94. https://doi.org/10.1016/S0029-5493(01)00433-2.

Sehgal, B.R., 2011. Nuclear Safety in Light Water Reactors: Severe Accident Phenomenology, first ed. Academic Press.

Shibazaki, H., Maruyama, Y., Kudo, T., Yuchi, Y., Chino, E., Nakamura, H., Hidaka, A., Hashimoto, K., 2000. Experimental study on effects of boric acid on aerosol revaporization in WIND project. In: JAERI - Conf 2000 - 015, pp. 225–230.

Soffer, L., Burson, S.B., Ferrell, C.M., Lee, R.Y., Ridgely, J.N., 1995. Accident Source Terms for Light-Water Nuclear Power Plants. Final Report. Nuclear Regulatory Commission, Washington, DC (United States). Div. Of Systems Technology. Funding organisation: Nuclear Regulatory Commission, Washington, DC (United States).

Stackelberg, M.V., Quatram, F., Dressel, J., 1937. Die Flüchtigkeit der Borsäuren mit Wasserdampf. Das System B2O3-Wasser. Zeitschrift für Elektrochemie und Angew. Phys. Chem. 43, 14–28. https://doi.org/10.1002/BBPC.19370430104.

Tanabe, F., 2011. Analysis of core melt accident in Fukushima daiichi-unit 1 nuclear reactor. J. Nucl. Sci. Technol. 48, 1135–1139. https://doi.org/10.1080/18811248.2011.9711800.

Vandeputte, R., Khiri, D., Lafont, C., Cantrel, L., Louis, F., 2019. Theoretical investigation of thermochemical properties of cesium borates species. J. Nucl. Mater. 517, 63–70. https://doi.org/10.1016/J.JNUCMAT.2019.01.036.